International Journal of Heat and Mass Transfer 95 (2016) 506–516

Contents lists available at ScienceDirect

International Journal of Heat and Mass Transfer

journal homepage: www.elsevier.com/locate/ijhmt

Numerical investigation of coalescence-induced droplet jumping on superhydrophobic surfaces for efficient dropwise condensation heat transfer

Yongpan Cheng [a,b], Jinliang Xu [a,*], Yi Sui [b]

[a] Beijing Key Laboratory of Multiphase Flow and Heat Transfer for Low Grade Energy, North China Electric Power University, Beijing 102206, China
[b] School of Engineering and Materials Sciences, Queen Mary University of London, Mile End Road, London E1 4NS, United Kingdom

ARTICLE INFO

Article history:
Received 27 July 2015
Received in revised form 7 November 2015
Accepted 21 November 2015

Keywords:
Droplet jumping
Multiphase flow
Condensation heat transfer
Diffuse interface method
Contact angle hysteresis

ABSTRACT

Dropwise condensation has much higher heat transfer efficiency than the filmwise condensation, hence it will be widely applied in power generation, waste heat recovery, refrigeration etc. The spontaneous coalescence-induced droplet jumping on superhydrophobic surfaces was an effective way to maintain highly efficient dropwise condensation. In our study, the coalescence-induced droplet jumping process was numerically studied through transient three-dimensional diffuse interface method. The effect of contact angle and its hysteresis, droplet size, viscosity and gravity on the jumping process was studied in details, energy conversions were also provided among the droplet surface energy, viscous dissipation, kinetic energy and gravitational energy. Our study showed that contact angle had negative effect on the jumping velocity, with the decreasing contact angle, both peak jumping velocities and radius range for droplet jumping would be reduced. For the capillary-inertial process the normalized droplet jumping velocity was at the order of 0.2. Although more than half of the released surface energy could be converted into the kinetic energy, only less than 10% of the released surface energy could be converted into the translational kinetic energy for droplet jumping. The contact angle hysteresis had significant effect on the droplet jumping, the larger advancing contact angle could help improve the droplet jumping velocity, while the lower receding contact angle could reduce the droplet jumping velocity. Our results might provide useful guideline for design of efficient dropwise condensation heat transfer through coalescence-induced droplet jumping on superhydrophobic surfaces.

1. Introduction

Condensation heat transfer is widely used in power generation, refrigeration, waste heat recovery etc. [1–3], and it has great significance in improving the energy utilization and relieving pollution problems. The condensation can be classified into dropwise and filmwise condensations [4]. In the filmwise condensation the condensate will spread into a thin film on the cooling surface, thus prevent the direct contact between the condensing vapor and sub-cooled surface, so the heat transfer will be deteriorated. Some measures have to be taken to improve the filmwise condensation, such as interrupted plates, flow pattern modulation etc. [5–8]. On the contrary, in the dropwise condensation the condensate will not wet the sub-cooled surfaces, its heat transfer efficiency can be one order higher than that of the filmwise condensation [9]. However, in order to maintain the stable and efficient dropwise condensation, the condensate should be removed quickly from the sub-cooled surfaces. At large diameter of condensate at the order of capillary length ($\lambda = \sqrt{\frac{\sigma}{\rho g}} = 2.7$ mm for water at 20 °C), the condensate can be removed with the aid of gravity, but droplet accumulation on the sub-cooled surface may hinder the nucleation frequency, resulting poor condensation heat transfer. In order to improve the heat transfer efficiency, the condensate therefore should be removed quickly, furthermore, the decreasing size of the departure droplet helps improve the heat transfer efficiency [10].

Boreyko and Chen [11,12] found that the condensate of 30 times smaller than the capillary length could jump from the superhydrophobic surfaces spontaneously without any external forces, and the resulting departure speed could be as high as 1 m/s. They also found that the kinetic energy for jumping came from the released surface energy, the jumping velocity followed the capillary-inertial law, which was proved on chilled

* Corresponding author. Tel.: +86 10 61772268.
E-mail address: xjl@ncepu.edu.cn (J. Xu).

http://dx.doi.org/10.1016/j.ijheatmasstransfer.2015.11.074
0017-9310/

Nomenclature

Bo	Bond number
C	volume fraction of liquid
e	energy, J
E^*	non-dimensional energy
f	free energy density, N/m^3
g	gravitational acceleration, m/s^2
h	height of droplet, m
M	mobility, m^4/(N s)
Oh	Ohnesorge number
p	pressure, Pa
Pe	Pelect number
r_0	droplet radius, m
Re	Reynolds number
t^*	non-dimensional time
u	velocity, m/s
U^*, V^*, W^*	non-dimensional velocity
V_0	droplet volume, m^3
x, y, z	coordinates, m
X^*, Y^*, Z^*	non-dimensional coordinates
α	constant, $6\sqrt{2}$
ε	thickness of interface, m
$\bar{\varepsilon}$	non-dimensional thickness of interface
ϕ	chemical potential, N/m^2
λ	capillary length, m
μ	viscosity, Pa s
$\bar{\mu}$	non-dimensional average viscosity, $\bar{\mu} = C + (1 - C)\mu_g/\mu_w$
θ	contact angle, degree
ρ	density, kg/m^3
ρ_d	density ratio
$\bar{\rho}$	non-dimensional average density, $\bar{\rho} = C + (1 - C)\rho_g/\rho_w$
σ	surface tension, N/m
τ	time constant
ψ	bulk energy density, N/m^3
Φ	viscous dissipation rate
ci	capillary-inertial
d	dissipation
g	gravity, gas
gc	gravitational center
j	jump
k	kinetic
s	surface
$trans$	translational
w	water

superhydrophobic surface, as well as the heated Leidenfrost surface. On the Leidenfrost surface, the droplet was suspended over the vapor layer because its temperature was above the boiling temperature. Dorrer and Ruhe [13] also found that the condensate could move quickly on the nano-micro scale superhydrophobic surfaces, leading to high condensation heat transfer. Tian et al. [14] fabricated the superhydrophobic surfaces with the closely packed ZnO nanoneedles, and achieved the efficient self-propelling of small-scale condensed microdrops, the droplets with diameters below 10 μm occupied more than 80% of the total drop number of residual condensates. Lv et al. [15] found the condensation and jumping relay of droplets on lotus leaf, and reported that the surface energy dissipation was the main reason controlling the critical size of jumping droplet. Miljkovic et al. [16] found that the condensation heat transfer could be enhanced by up to 30% due to the resulting coalescence-induced droplet jumping. Liu et al. [17] adopted two-dimensional Lattice Boltzmann Method (LBM) to simulate the self-propelled jumping of droplets after coalescence on a superhydrophobic surface, as well as the dropwise condensation of vapor along vertical hydrophobic flat plates [18]. They [19] also studied the morphological effects on the self-propelled jumping of droplets on textured superhydrophobic surfaces, and revealed that there was optimal roughness spacing for maximum jumping velocity, their findings could be used to explain the large differences in measured jumping velocities of small droplets on hierarchical textured and nanostructured surfaces in the experiments. With three-dimensional multi-relaxation-time pseudopotential Lattice Boltzmann method, Shi et al. [20] studied the coalescence-induced droplet jumping on superhydrophobic complex textured surface, and revealed the effect of surface conical posts, droplet number and radius, the surface wettability on the droplet jumping. Nam et al. [21] conducted full three-dimensional numerical simulation on the dynamic analysis of coalescence-induced jumping on superhydrophobic surface, and they found that 40–60% of the released surface energy could be converted into total kinetic energy before the coalesced droplets detached from the substrate. Furthermore, they extended the study to oil-infused superhydrophobic and hydrophobic surfaces [22], and they found that 30% and 22% of released surface energy could be converted into kinetic energy respectively. After detachment, the total kinetic energy could be converted into viscous dissipation energy, gravitational energy. Liu et al. [23] conducted the three-dimensional phase field simulation of coalescence of two identical spherical drops on a superhydrophobic surface with contact angle 180°, and proved that the droplet jumping resulted from the counter-action of the substrate to the impingement of the liquid bridge between coalescencing drops, the jumping velocity was nearly constant at around 0.2 when scaled by the capillary-inertial velocity. In the heated Leidenfrost surfaces, the droplets were not in contact with the surface, instead they were separated from the surface by a thin vapor layer, hence the contact angle could be considered as ideal 180°, Liu et al. [24] the measured jumping velocity at the scale of 0.2 for coalesced droplet on Leidenfrost surfaces, which was quite close to value on the superhydrophobic surfaces. On both surfaces, the scaled jumping velocity of 0.2 indicated that around 4% of released energy was converted into translational kinetic energy. Through experiments Enright et al. [25] found that at the droplet diameter of 10 μm the droplet jumping velocity could be as high as 1.4 m/s, but only less than 6% of the released surface energy could be converted into translational kinetic energy. Their values on the energy conversion ratios were much lower than that obtained by Nam et al. [21,22], because they focused on the translational kinetic energy after droplet detachment from the substrate, which were closely related to the droplet jumping. But Nam et al. [21,22] focused on the total kinetic energy before droplet detachment, it would be further converted into other forms of energy after detachment, and only a small fraction of total energy was the translational energy. However, they only focused on the coalescence-induced droplet jumping within a narrow range of contact angles and droplet radius.

The effect of the contact angles on the coalescence-induced droplet jumping was seldom addressed due to the singularity behavior at the contact lines. Liu et al. [23] avoided this problem by assuming the contact angle as 180°, Nam et al. [21,22] tried to resolve this

problem by adopting the Navier-slip model in their simulations. In our study we adopted the geometric formulation to approximate the contact line and studied the effect of contact angle, the reliability and accuracy had been proved by Ding and Spelt [26]. Our work was the extension of their work, the effect of contact angles and droplet radius on the coalescence-induced droplet jumping was studied in the wider range, and the energy conversions during the process was also explored in details. Furthermore, when the droplet advanced or recede along the solid substrate, the contact angle hysteresis had great effect on the dynamics of droplet, especially for the coalescence-induced droplet jumping, this was also objective of our study.

In the following sections the physical model and numerical formulation would be provided first, followed by the detailed studies of jumping process of coalesced droplets under different contact angles and droplet diameters. After that, the energy conversion during the coalescence would be provided as well as the effect of contact angle hysteresis on the jumping process. Finally some conclusions would be drawn, which might be useful for design of efficient condensation heat transfer surface through coalescence-induced droplet jumping.

2. Physical model and mathematical formulation

Fig. 1 shows the schematic diagram of dropwise condensation in the condenser, with vapor flowing inside and the coolant flowing outside. When the vapor released heat to the cooling wall, it would be condensed into the droplets. When the two adjacent droplets coalesced, the excess surface energy would be released due to reduction of surface area. Due to the counter action of the substrate upon impingement of liquid bridge for coalescing droplets, the droplet would jump up from the substrate. The two droplets were assumed as equal sizes, the original radius of the droplet was r_0 with contact angle θ. In our simulation, the diffuse interface model [27] was adopted to study the coalescence-induced jumping process of droplets. In this model the divergence-free velocity field was derived from the mass conservation law of binary mixture, thus it was applicable for fluids with large density and viscosity ratios, the interface was captured from the convective Cahn–Hilliard equation.

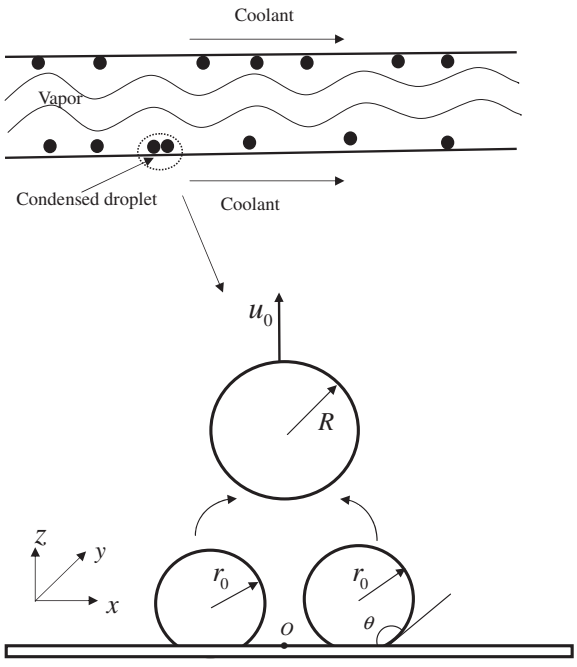

Fig. 1. Schematic of coalescence-induced jumping on superhydrophobic surfaces.

According to capillary-inertial scaling, the following characteristic velocity was defined:

$$u_{ci} = \sqrt{\frac{\sigma}{\rho r_0}}. \tag{1}$$

The corresponding characteristic time scale was

$$\tau_{ci} = \frac{r_0}{u_{ci}} = \sqrt{\frac{\rho r_0^3}{\sigma}}. \tag{2}$$

In order to evaluate the relative importance of different forces, the following dimensionless numbers were adopted:

The Ohnesorge number Oh denotes the relative importance of viscous effect versus capillary-inertial effect. When the viscous length scale is 10 nm based on $Oh \sim 1$, the capillary-inertial scaling is no longer observed.

$$Oh = \frac{\mu_w}{\sqrt{\rho_w \sigma r_0}}. \tag{3}$$

The Bond number denotes the relative importance of gravitational force over the surface tension. When the length scale is 1 mm based on $Bo \sim 1$, the gravitational force plays an important role, the capillary-inertial scaling is also not observed

$$Bo = \frac{(\rho_w - \rho_g) g r_0^2}{\sigma}. \tag{4}$$

Therefore, when the droplet size is at the nano-scale or millimeter-scale, the coalescence-induced jumping of droplet will be affected due to viscous or gravitational effects, the detailed analysis will be provided in the following section.

The mass-averaged velocity was defined as follows:

$$U_j = \frac{\int_\Omega C \rho_w U_j d\Omega}{\int_\Omega C \rho_w d\Omega}. \tag{5}$$

The characteristic energy was based on the order of surface energy σr_0^2, therefore the normalized governing equations were shown below:

Continuity equation

$$\nabla \cdot \vec{U}^* = 0. \tag{6}$$

Momentum equation

$$\bar{\rho}\left[\frac{\partial \vec{U}^*}{\partial t^*} + \vec{U}^* \cdot \nabla \vec{U}^*\right] = -\nabla \bar{p} + \frac{1}{Re}\nabla \cdot [\bar{\mu}(\nabla \vec{U}^* + \nabla \vec{U}^{*T})] + \phi \nabla C - Bo\vec{k}. \tag{7}$$

Interface tracking

$$\frac{\partial C}{\partial t^*} + \vec{U}^* \cdot \nabla C - \frac{1}{Pe}\nabla \cdot (M \nabla \phi) = 0, \tag{8}$$

here $Re = \frac{\rho u_{ci} r_0}{\mu}$, $Pe = \frac{u_{ci} r_0}{M\phi}$, $\phi \nabla C$ and $Bo\vec{k}$ were terms caused by surface tension and gravitational terms respectively.

The coupling between the continuity Eq. (6) and momentum Eq. (7) was solved with the standard projection method [27]. First, a viscous solve was performed using Adams–Bashforth for the advection term and Crank-Nicolson for the diffusion term, thus the intermediate velocity could be obtained, then it would be updated through pressure correction enforced by the continuity equation. For the Cahn–Hilliard interface tracking Eq. (8), the transient term was discretized with split semi-implicit method, the advection term was discretized with a fifth-order weighted essentially non-oscillatory (WENO) scheme. All the spatial discretizations were performed with the second-order central difference scheme.

The interface was assumed to be driven through convection or diffusion driven by chemical potential gradients [28]. Based on the volume fraction C and its gradient, a free energy density model for immiscible isothermal two-phase fluids was used

$$f = \frac{1}{2}\varepsilon\sigma\alpha|\nabla C|^2 + \varepsilon^{-1}\sigma\alpha\psi(C). \tag{9}$$

The first term represented the excess free energy due to the inhomogeneous distribution of volume fraction, the second term represented $\psi(C) = \frac{1}{4}C^2(1-C)^2$ was the bulk energy density.

The governing equations were discretized with finite difference method on staggered grid to ensure the coupling between pressure and velocity, then they were solved with projection method. Due to the symmetry in horizontal x and y direction, only 1/4 of the two merged droplets (half of a droplet) were simulated with the dimensionless volume of $4 \times 4 \times 6$, as shown in Fig. 2. The lower boundary ($z = 0$) was the superhydrophobic solid surface. At $x = 0$ or $y = 0$, the symmetric boundary was applied, the other boundaries were free boundary conditions. In order to introduce the effect of contact angle of superhydrophobic surfaces on the coalescence-induced process, the geometric formulation was used to compute the contact angle θ, as shown below [26]

$$\tan\left(\frac{\pi}{2} - \theta\right) = \frac{-\vec{n}\cdot\nabla C}{|\nabla C - (\vec{n}\cdot\nabla C)\vec{n}|}. \tag{10}$$

At the contact line, $\vec{n}$ intersected the solid substrate at an angle of $\frac{\pi}{2} - \theta$. At initial stage the two adjacent droplets rest in the static state on the solid substrate with the prescribed contact angle θ. During the coalescence-induced jumping process, the dynamic contact angle might vary greatly. For simplification the advancing contact angle and receding contact angle were assumed to be the same as the static contact angle in most of the studies. But in the last section, the effect of contact angle hysteresis on the droplet jumping process was provided. After coalescence the droplets would move towards each other in x direction and started to jump up in z direction.

3. Results and discussion

3.1. Numerical validation

The properties of the droplet was taken as water at 20 °C, the density and viscosity ratio between the surrounding gas and water was $\rho_g/\rho_w = \mu_g/\mu_w = 0.05$. It had been tested that if this value was further reduced to 0.01, it would exert little effect on the jumping

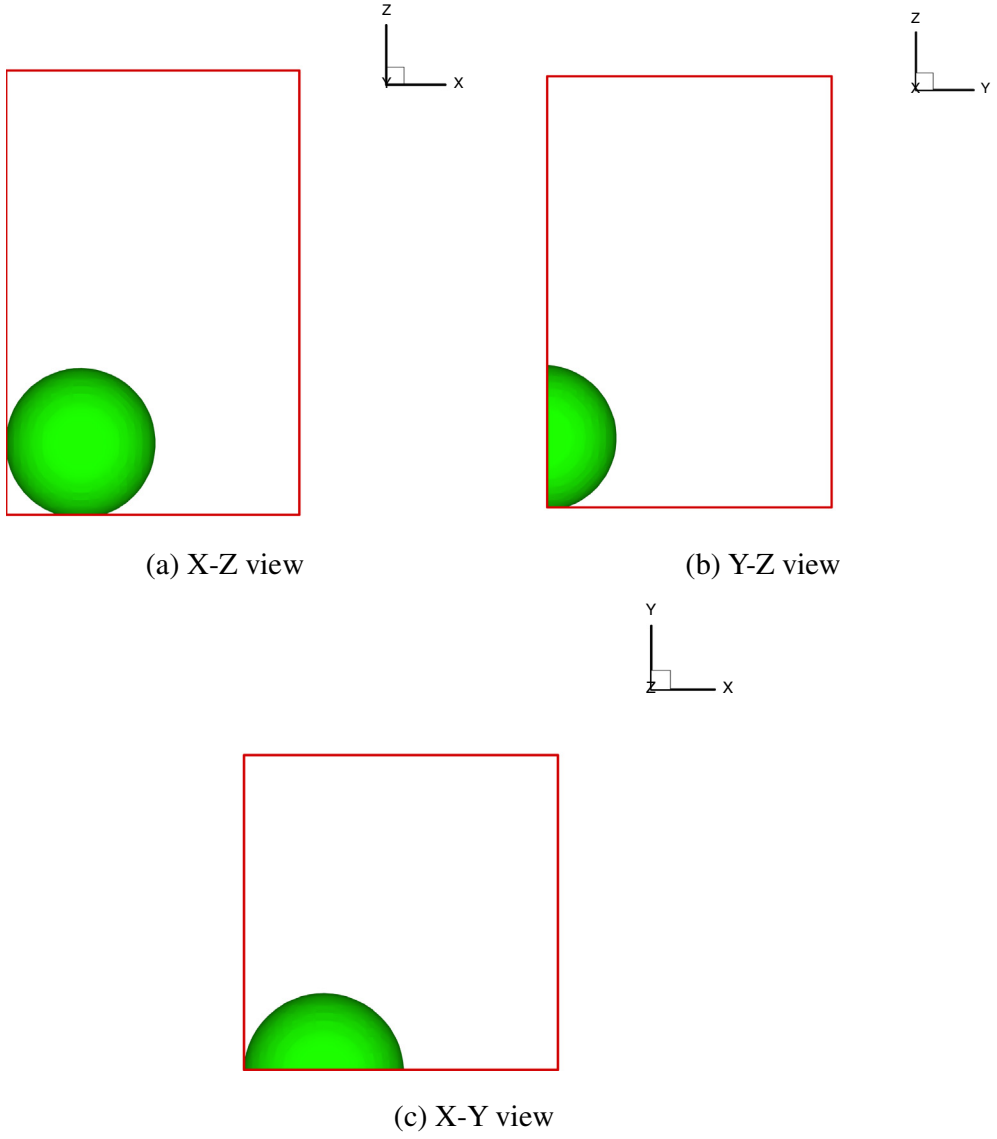

Fig. 2. Computational domain for numerical simulation (1/4 of domain was selected due to symmetry in x and y directions. Two adjacent droplets coalesced in x direction and jumped up in z direction).

process as well as the energy conversions; hence in order to stabilize the convergent process, the value 0.05 was taken as the density and viscosity ratio. After the validation study the capillary width was taken as $\varepsilon = 0.05$, the grid number was $61 \times 61 \times 91$ and time step was 1.0×10^{-4}.

For the two adjacent droplets with equal radius r_0, if the contact angle was 180° under ideal situation, the released energy upon coalescence would be [23]

$$\Delta e = 4\sigma\pi r_0^2(2 - 2^{2/3}). \tag{11}$$

If all the released surface energy was converted into the translational kinetic energy, the vertical jumping velocity would be

$$u_j = \sqrt{2\Delta e/(8/3\rho\pi r_0^3)} = 1.11u_{ci}. \tag{12}$$

In order to validate our developed numerical model, the simulated results were compared with the available experimental data [24] and numerical data [23,25]. In Fig. 3(a) the transient vertical axial length of the merged droplet was compared with the experimental data from Liu et al. [24], their experiment was carried out on Leidenfrost surfaces. For the convenience of comparison, the vertical height and time were normalized with the droplet radius and characteristic time in Eq. (2). Because of the prescribed overlapping of two droplets before coalescence, the initial axial length at $t = 0$ was not zero. Due to the rotated view from the high-speed camera in experiment by Liu et al. [24], the axial length could not be assessed immediately after coalescence, so the reliable data started from around $t = 0.54$. During the range of time from 0.54 to 3.2, the predicted transient variations agreed quite well with the experimental data, furthermore, the numerical studies showed that maximum vertical height occurred at around $t = 2.7$, as measured through the experiment.

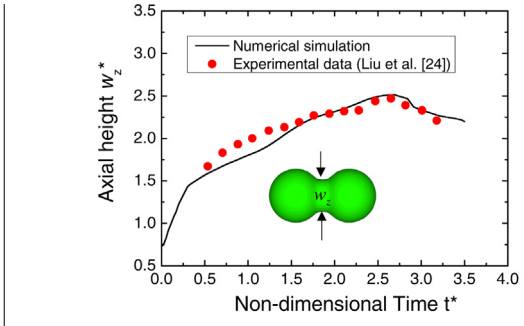

(a) Simulated and measured vertical axial length at $r_0 = 0.38$mm for water droplet at t=100°C

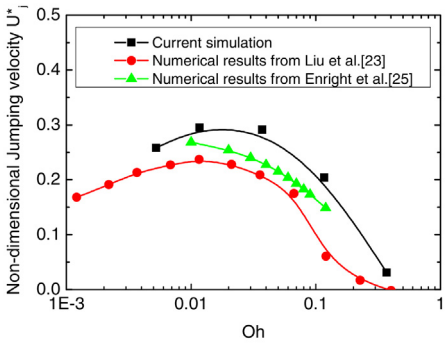

(b) The jumping velocity of merged droplets over Ohnesorge number at θ=180°

Fig. 3. Comparison of current numerical results with available data (Solid lines were fitted curves).

Liu et al. [23] and Enright et al. [25] had simulated the coalescence-induced droplet jumping process on the ideal flat surface with contact angle 180°, our simulated jumping velocities were compared with their results. It could be found that for moderate Ohnesorge number in the capillary-inertial process, our predicted jumping velocity agreed well with their results, all of the velocities ranged from 0.2 to 0.3. The variation trends of the jumping velocities from our simulation and their results were also consistent, i.e. with the increasing droplet size or decreasing Ohnesorge number, the jumping velocity increased first due to decreasing viscous effect at small droplet size, after reaching the peak it started to decrease due to the increasing inertial effect at moderate droplet size, and increasing gravitational effect at large droplet size (large Bond number).

3.2. Morphological variations during capillary-inertial jumping process

Fig. 4 shows the coalescence-induced jumping process at contact angle $\theta = 150°$ and $r_0 = 100$ μm At this radius the Ohnesorge number $Oh = 0.0118$ and Bond number $Bo = 0.00135$, hence the capillary-inertial process dominated, viscous and gravitational effect only played a secondary role. At $t = 0$, the two adjacent droplets were overlapped with the diffuse interface, because the relative large curvature near the liquid bridge, the surface tension force of the droplets would drive the flow towards the liquid bridge, then the bridge became wider in vertical direction. At $t = 0.4$, it reached the substrate, due to the repulsive forces by the substrate, the droplets started to move upward against the substrate. It was noted that the topological configuration of the droplet was three-dimensional, the reduction of the footprint in one view might be compensated with the increase in another view due to mass conservation. After $t = 0.6$ the merged droplet started to shrink in x direction and continued to move upward in z direction. The contact area between the merged droplet and the substrate was decreasing until zero at $t = 3.20$, at this point the droplet departed from the substrate. Due to the inertial effect the droplet maintained an upward motion and continued to oscillate between oblate and prolate. The top view of the merged droplets was also shown in Fig. 4, in y direction there was no confinement for the droplet, the topology and motion were kept symmetrical due to the symmetry of droplet.

3.3. Transient variations of vertical velocity

3.3.1. Effect of droplet radius

During the capillary-inertial process for the coalescence-induced jumping, the viscous effect controlled the process at small droplet radius due to large Ohnesorge number, while the gravitational effect controlled the process at large droplet radius due to large Bond number. In Fig. 5(a) the transient variations of average vertical velocities were shown with the droplet radius ranging from 100 nm to 0.5 mm. It would be found that when the droplet radius was 100 nm, the maximum vertical velocity was around 0.11, which was so low that the coalesced droplet could not jump upward from the substrate. If the droplet radius was increased to 10 μm, due to reduced viscous dissipation, more excess surface energy could be released into kinetic energy, hence the maximum vertical velocities could be as high as 0.28. When the droplet radius was increased to 100 μm, the maximum vertical velocity was increased to around 0.29. It was noted that although there was limited difference for the normalized vertical velocities at the droplet radius of 10 μm and 100 μm, the absolute maximum vertical velocity at $r_0 = 100$ μm was only around 1/3 of that $r_0 = 10$ μm because the characteristic velocity was in inverse proportional to the square root of the radius, as seen in Eq. (1). If the droplet radius

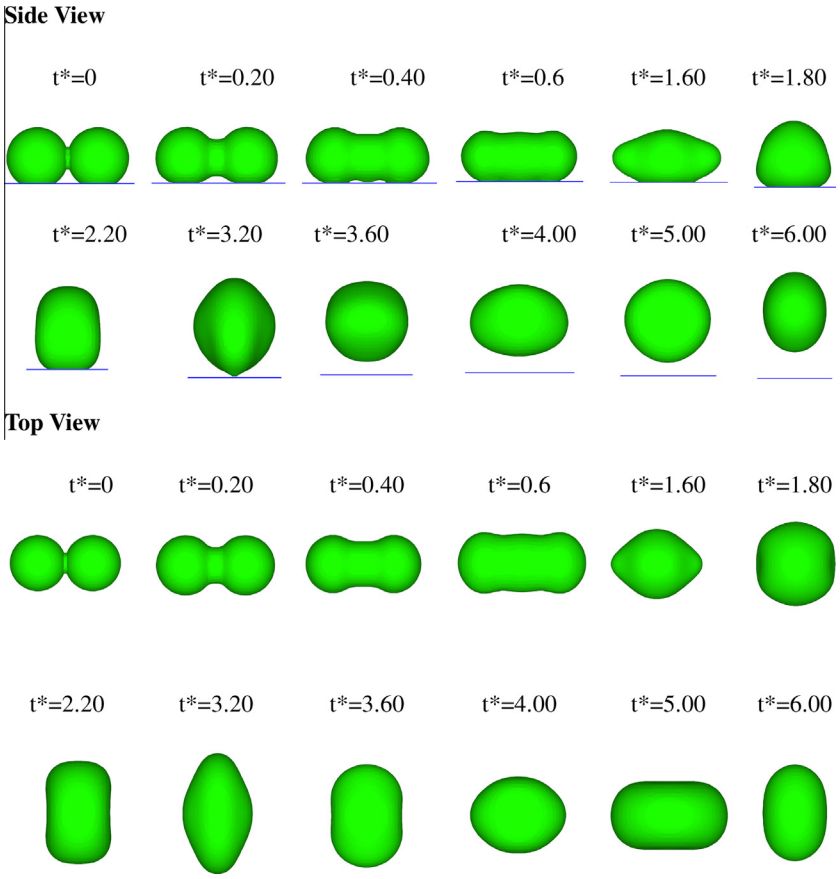

Fig. 4. The snapshots of coalescence and jumping process of two droplets at $\theta = 150^{\circ}$, $r_0 = 100$ μm ($Bo = 1.35 \times 10^{-3}$, $Oh = 1.18 \times 10^{-2}$).

was increased further to 0.5 mm, after coalescence the coalesced droplet would move upward due to the impingement against the substrate, but quickly it would move downward due to the gravitational force, hence the overall vertical droplet velocities would drop quickly from positive to negative values. This phenomenon could be explained from energy conversions in the later section.

3.3.2. Effect of contact angles

For the real superhydrophobic surfaces the contact angle would not be ideal 180°, hence it was necessary to study the effect of contact angle on the vertical velocities, as seen in Fig. 5(b). When the contact angles varied from 180° to 120°, there was limited difference in the vertical velocities during the initial coalescence process. However, after reaching the maximum velocities, the vertical velocities at 150° and 180° would decrease mildly with the positive values, indicating that at these two contact angles the coalesced droplet could jump up from the substrate. However, when the contact angles were reduced to 140° or even 120°, the vertical velocities would oscillate strongly between the positive and negative values, which meant that the coalesced droplet could not jump up.

3.4. Jumping velocities under different contact angles

From the transient variations of vertical velocities in Fig. 5, the jumping velocity could be extracted at which point the merged droplet departed from the substrate. It was noted that the jumping velocity occurred later than the maximum vertical velocity. Fig. 6 shows the jumping velocities under different contact angles. It was found that the contact angle had significant effect on the droplet jumping velocity. At contact angle $\theta = 180^{\circ}$, the maximum jumping velocity was around 0.29, while when the contact angle was reduced further to $\theta = 150^{\circ}$, the maximum jumping velocity was only 0.22.

For all three contact angles, under small droplet radius the jumping velocity was reduced with decreasing droplet radius, because the viscous effect was dominant, the released excess surface energy was quickly dissipated through viscous dissipation, and little energy was converted into the kinetic energy. However, under large droplet radius the jumping velocity was also reduced with increasing droplet radius, because the gravitational effect was dominant, a fraction of the excess surface energy was converted into the gravitational potential energy, thus less kinetic energy was obtained. It could also be found that the lower limit of the droplet radius for jumping was increased dramatically from ~10 nm at $\theta = 180^{\circ}$ to ~ 10 μm at $\theta = 150^{\circ}$.

3.5. Energetics of droplet jumping

During the coalescence-induced jumping process, the surface energy E_s would be converted into the kinetic energy E_k, gravitational energy E_g and viscous dissipation E_d. In order to reveal the process, the energy conversions among them were studied in details as follows. It was noted that in the following definitions all the variables were dimensionless, and the energy was normalized with σr_0^2.

The surface energy came from the free energy density model in our simulation

$$E_{s,s}^{*} = \int_{\Omega^{*}} \left(\frac{1}{2}\bar{\varepsilon}\alpha|\nabla C|^2 + \frac{\alpha}{4\bar{\varepsilon}} C^2(1-C)^2 \right) d\Omega. \tag{13}$$

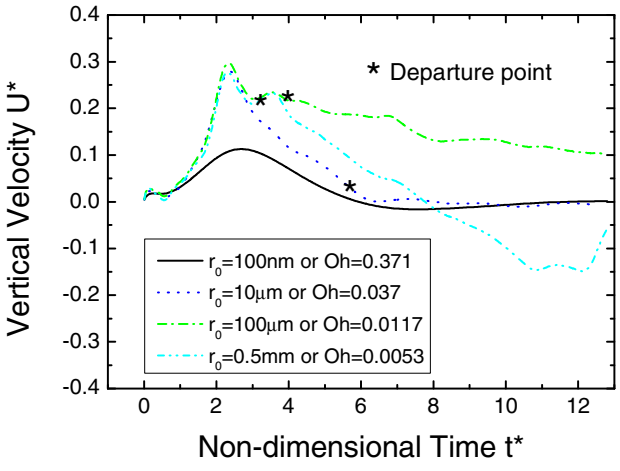

(a) Effect of droplet radius at θ=150°

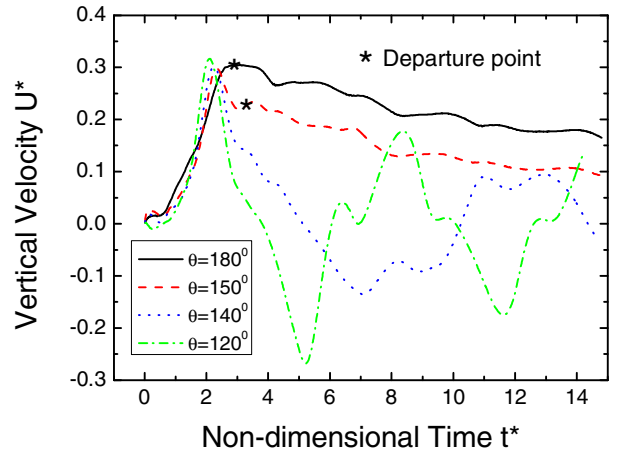

(b) Effect of contact angle at $r_0 = 100\,\mu m$ (Oh=0.0117)

Fig. 5. Transient variation of mass-average vertical velocities.

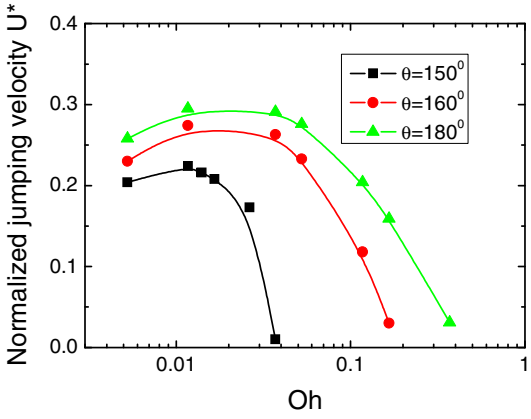

(a) Normalized velocity

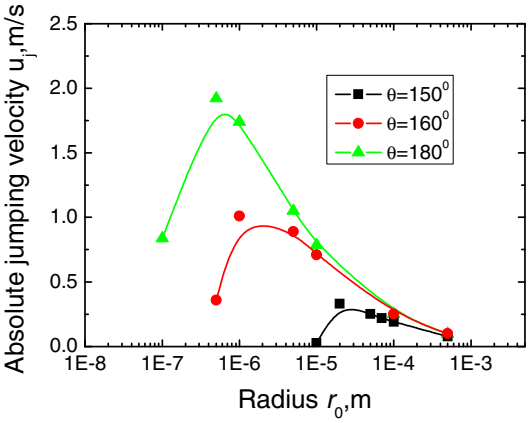

(b) Absolute velocity

Fig. 6. Dependence of jumping velocity on droplet radius under different contact angles. (Solid lines were fitted curves.)

The first term in the bracket was the excess free energy due to the inhomogeneous distribution of volume fraction C, the second term was the bulk energy density. Ω was the whole computational domain including the liquid droplet and gas around it.

The total kinetic energy was defined as

$$E^*_{k,total} = \int_{\Omega^*} \frac{1}{2}[C + (1-C)\rho_d]|U^*|^2 d\Omega. \tag{14}$$

The translational kinetic energy in vertical jumping direction was defined as

$$E^*_{k,trans} = \int_{\Omega^*} \frac{1}{2}[C + (1-C)\rho_d]|U^*_z|^2 d\Omega. \tag{15}$$

The gravitational energy was related to Bond number and the height increase relative to the original location

$$E^*_g = Bo\Delta Z^*. \tag{16}$$

The dissipation function for the continuum fluid was defined as

$$\Phi^* = 2\left(\frac{\partial U^*}{\partial X^*}\right)^2 + 2\left(\frac{\partial V^*}{\partial Y^*}\right)^2 + 2\left(\frac{\partial W^*}{\partial Z^*}\right)^2 + \left(\frac{\partial V^*}{\partial X^*} + \frac{\partial U^*}{\partial Y^*}\right)^2 + \left(\frac{\partial W^*}{\partial Y^*} + \frac{\partial V^*}{\partial Z^*}\right)^2 + \left(\frac{\partial U^*}{\partial Z^*} + \frac{\partial W^*}{\partial X^*}\right)^2. \tag{17}$$

The viscous dissipation was related to the Ohnesorge number, and was the time integration of dissipation function as

$$E^*_d = \int_0^{\tau^*} [C + (1-C)\rho_d] Oh\Phi^* dt. \tag{18}$$

For a spherical cap with an apparent contact angle θ, theoretically the normalized surface energy is [29]

$$E^*_{s,t} = \pi(2 - 2\cos\theta - \cos\theta\sin^2\theta). \tag{19}$$

The original surface energy before droplet coalescence at $\theta = 150°$ in our simulation should be $\frac{1}{2}\pi(2 - 2\cos\theta - \cos\theta\sin^2\theta) =$ 6.20, after coalescence the surface energy of droplet at equilibrium state should be 4.95.

3.5.1. Energy conversions under different droplet radius

Fig. 7 shows the transient variation of energy during the coalescence-induced jumping process. It could be found that the calculated initial surface energy under different droplet radius was around 6.06, quite close to the theoretical value 6.20. At $r_0 = 100$ nm the released surface energy was converted into kinetic energy and viscous dissipation. Due to the large viscosity, the kinetic energy would be dissipated very quickly, so the merged droplet would rest on the substrate soon. The maximum kinetic energy was around 0.1, which was a little fraction of the excess surface energy, and finally it was dissipated through viscous dissipation.

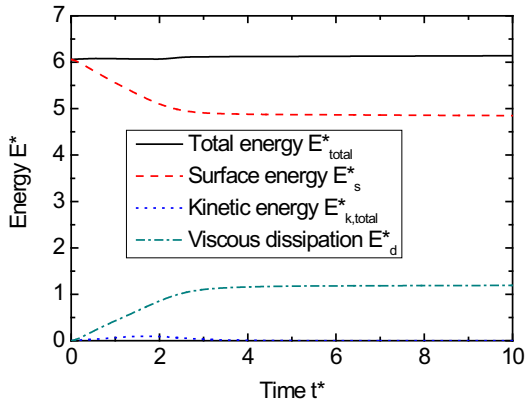

(a) $r_0 = 100$ nm (Oh=0.373)

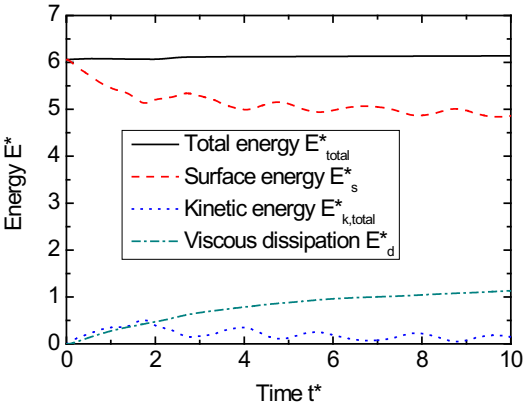

(b) $r_0 = 100\mu$m (Oh=0.0117)

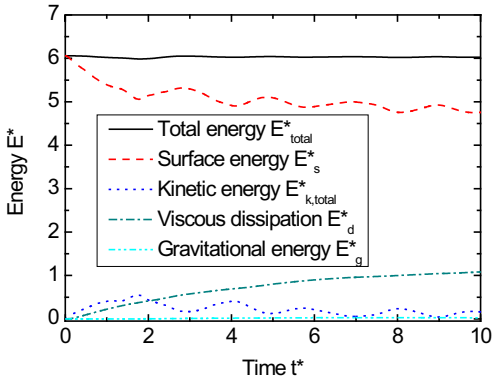

(c) $r_0 = 0.5$ mm (Oh=0.0053)

Fig. 7. The transient variations of energy during the coalescence-induced jumping process of droplet at $\theta = 150^\circ$.

At $r_0 = 100$ μm, it could be found that the excess surface energy was converted into the kinetic energy, then the merged droplet started to jump up from the substrate. The maximum kinetic energy was around 0.5, which accounted for almost half of the excess surface energy. With the maximum kinetic energy, the ideal velocity should be around 0.7, while the actual jumping velocity was only around 0.22, which was only around one third of the ideal velocity. The large discrepancy could be explained from the following two aspects, as seen in Fig. 8, in this figure the transient

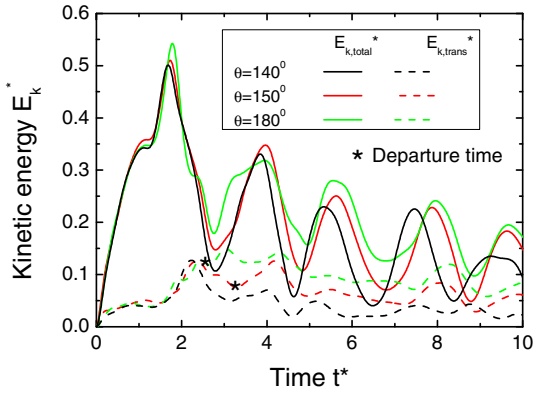

Fig. 8. The transient variations of the vertical and total kinetic energy under different contact angles at $r_0 = 100$ μm ($Oh = 0.0117$).

variations of the translational vertical and total kinetic energy are provided under different contact angles. (1) The maximum kinetic energy and jumping velocity upon droplet coalescence did not occur at the same time. For example, the maximum kinetic energy occurred at around $t = 1.8$ for contact angle $\theta = 150^\circ$ and 180°, while the droplet jumping occurred at $t = 3.20$ and $t = 2.55$ respectively. (2) The kinetics for droplet jumping came from the vertical kinetic energy only, while from Fig. 8 it could be found that the maximum translational kinetic energy was less than 20% of the maximum total kinetic energy, i.e. less than 10% of the excess surface energy. It meant that most of the kinetic energy was converted into the oscillations of the droplets, and would not contribute to the droplet jumping. This result was consistent with the findings from Nam et al. [21,22], Liu et al. [23,24] and Enright et al. [25] on the energy conversions.

3.5.2. Energy conversions under different contact angles

From the analysis above, it could be found that the contact angles had significant influence on the coalescence-induced droplet jumping process. For detailed analysis the transient energy variations were provided at three typical contact angles, namely at $\theta = 140^\circ$, 150°, 180°. It was noted that at $\theta = 140^\circ$, the coalesced droplet could not jump up.

3.5.2.1. Released surface energy. Fig. 9 shows the transient variations of the released surface energy under three different contact angles. At the initial stage of $r_0 = 100$ nm, the released surface energy decreased greatly, then approached almost a constant after $t = 3.0$, the coalesced droplet came to rest on the substrate because of the strong viscous effect. At larger droplet radius, the released surface energy decreased with the oscillations, this was caused by the variations of the morphology of coalesced droplet, as seen in Fig. 4. After coalescence the droplet would oscillate between the oblate and prolate, leading to the oscillations of the released surface energy.

3.5.2.2. Viscous dissipation. Viscous dissipation played an important role in coalescence-induced droplet jumping. Fig. 10 shows the transient variations of viscous dissipations under three different contact angles. At small droplet radius $r_0 = 100$ nm, all the released surface energy would be converted into the viscous dissipation quickly, hence, contrary to the variation trend of released surface energy, the viscous dissipation would increase quickly at the initial stage and then approach an constant. While at large droplet radius, the viscous dissipation would increase consistently because of the dynamic movement of the coalesced droplet.

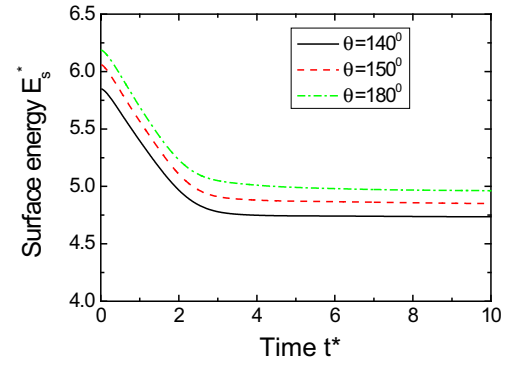

(a) $r_0 = 100\text{nm}$ (Oh=0.373)

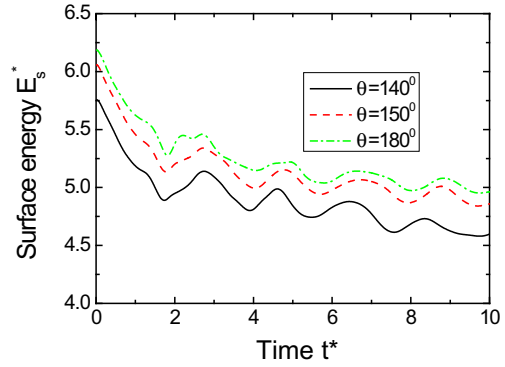

(b) $r_0 = 100\mu\text{m}$ (Oh=0.0117)

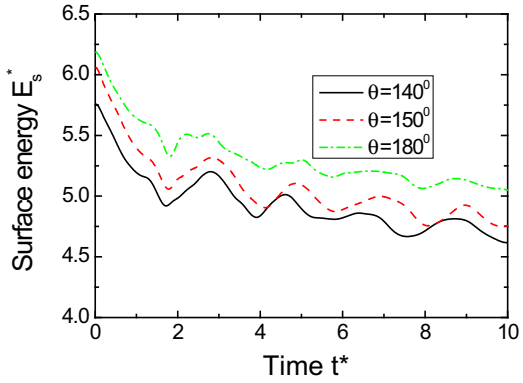

(c) $r_0 = 0.5\text{mm}$ (Oh=0.0053)

Fig. 9. Transient variations of surface energy under different contact angles.

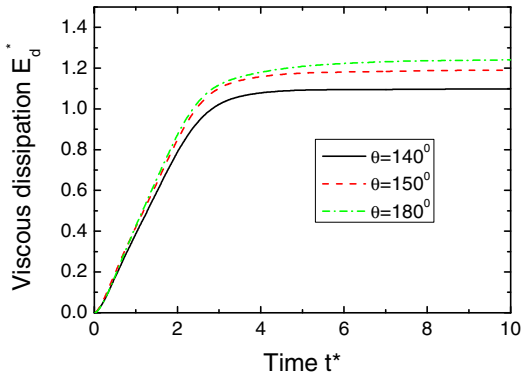

(a) $r_0 = 100\text{nm}$ (Oh=0.373)

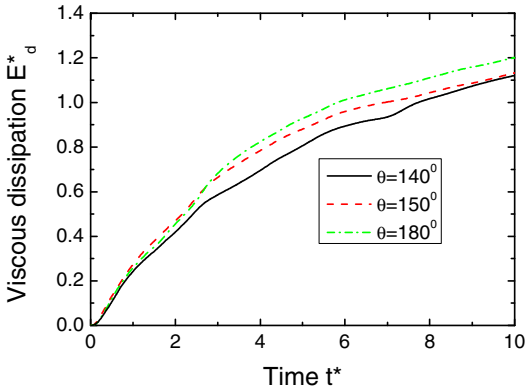

(b) $r_0 = 100\mu\text{m}$ (Oh=0.0117)

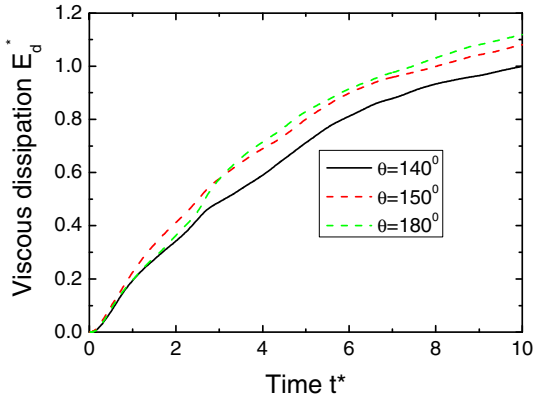

(c) $r_0 = 0.5\text{mm}$ (Oh=0.0053)

Fig. 10. Transient variations of viscous dissipations under different contact angles.

3.5.2.3. Kinetic energy. Fig. 11 shows the transient variations of the translational kinetic energy under three different contact angles, instead of the total kinetic energy, because the translational kinetic energy was directly related to the jumping of the coalesced droplet. It was found that at small droplet radius $r_0 = 100$ nm, only a very small fraction of kinetic energy could be obtained, and quickly they would come to zero due to strong viscous effect. At large droplet radius $r_0 = 100$ μm and 0.5 mm, the translational kinetic energy was quite higher than that at small droplet radius. It was noted that at $\theta = 140^\circ$, the translational kinetic energy dropped quickly after reaching the maximum, because at this contact angle, the coalesced droplet could not jump up.

3.5.2.4. Gravitational energy. When the droplet radius was large, the gravitational energy would have great effect on the droplet jumping. Because at the droplet radius $r_0 = 100$ nm and 100 μm, the gravitational energy was negligible, only the transient variation of gravitational energy at $r_0 = 0.5$ mm was provided in Fig. 12. It was noted that the gravitational energy was directly related to the height increase of droplet, as at $\theta = 140^\circ$ the coalesced droplet could not jump up, its gravitational energy would decrease greatly to almost zero after reaching the maximum. On the contrary, at $\theta = 150^\circ$ and 180°, the gravitational energy would increase rapidly first because the coalesced droplet could jump up.

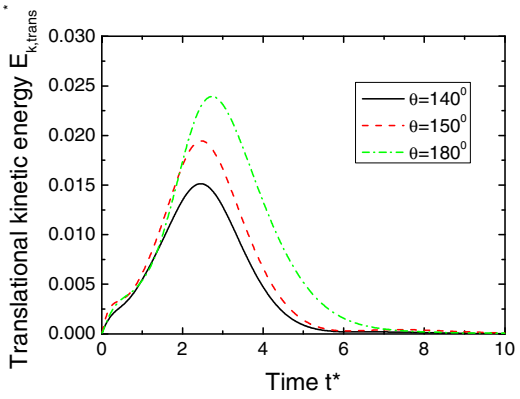

(a) $r_0 = 100\text{nm}$ (Oh=0.373)

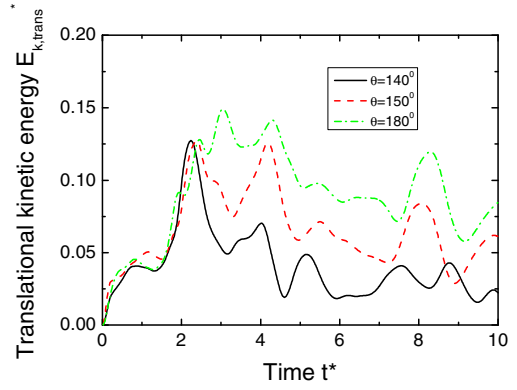

(b) $r_0 = 100\mu\text{m}$ (Oh=0.0117)

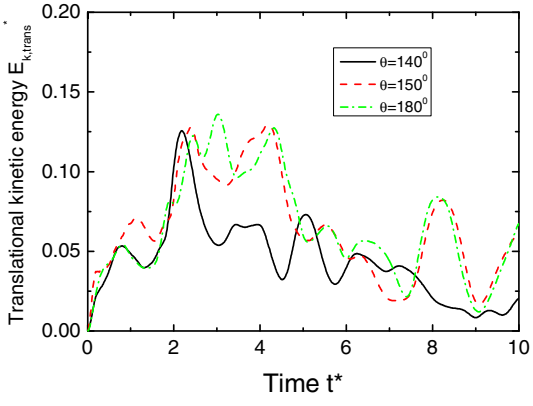

(c) $r_0 = 0.5\text{mm}$ (Oh=0.0053)

Fig. 11. Transient variations of translational kinetic energy under different contact angles.

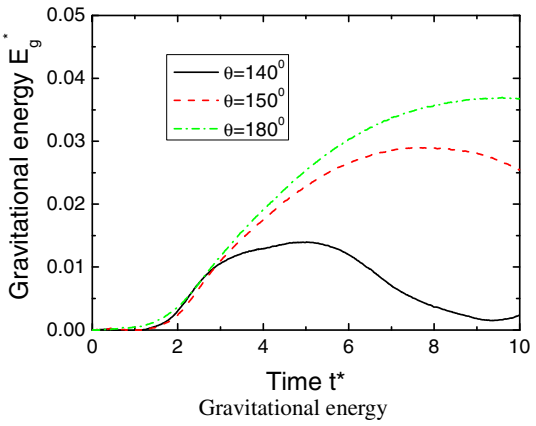

Gravitational energy

Fig. 12. Transient variations of gravitational energy under different contact angles at $r_0 = 0.5$ mm (Oh = 0.0053).

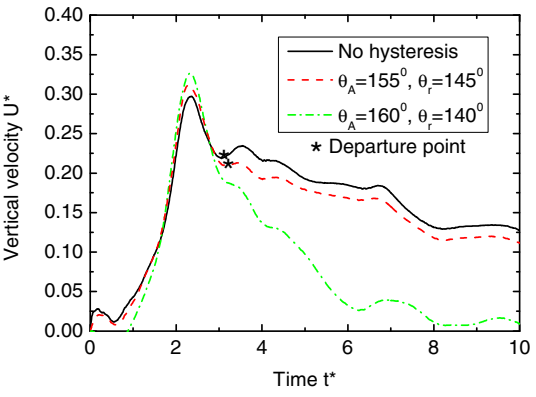

(a) Static contact angle $\theta = 150^0$

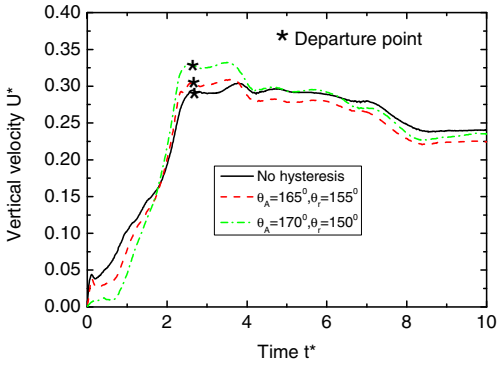

(b) Static contact angle $\theta = 160^0$

Fig. 13. Effect of contact angle hysteresis on the transient vertical velocity at $r_0 = 100$ μm (Oh = 0.0117).

3.6. Effect of contact angle hysteresis on the jumping process

In the previous studies above, the static contact angle was assumed, however, in the interaction between the droplet and solid substrate, the contact angle hysteresis played an important role. Fig. 13 shows the effect of contact angle hysteresis on the vertical velocity during the coalescence-induced droplet jumping with the constant static angle at $r_0 = 100$ μm. It could be found that the advancing contact angle could promote the droplet jumping, while the receding contact angle could defer the droplet jumping. The dynamics of the droplet jumping was determined by the competing effect of the advancing contact angle and receding contact angle. At the low static angle $\theta = 150°$, it could be found the receding contact angle played a more important role than the advancing contact angle. When the receding contact angle decreased, the jumping velocity would also decrease, and if the receding contact angle was lower than 140°, the coalesced droplet could not jump up. At high static angle $\theta = 160°$, it could be found that the advancing contact angle played a more important role, and the increasing advancing contact angle could promote the jumping velocity of coalesced droplet.

4. Conclusions

The diffuse interface method was adopted to simulate the coalescence-induced jumping process of two adjacent droplets with equal sizes, the effect of contact angles, droplet size, viscous and gravitational effects on the droplet jumping was investigated in details. The energy conversions among surface energy, viscous dissipation, kinetic energy and gravitational energy were provided. The main conclusions were summarized as follows:

1. Contact angle had negative effect on the jumping velocity, both peak jumping velocities and radius range for droplet jumping would be reduced when the contact angle was decreased.
2. At contact angle $\theta = 150^{\circ}$, for the capillary-inertial process the normalized droplet jumping velocity was at the order of 0.2. If the droplet radius was reduced, the jumping velocity would decease due to the greater viscous effect; While if the droplet radius was increased, the jumping velocity would also decrease due to the greater gravitational effect.
3. For the capillary-inertial process at $r_0 = 100$ μm, up to 50% of the excess energy could be converted into the kinetic energy, but only less than 10% of the excess energy could be converted into the translational energy for droplet jumping.
4. The contact angle hysteresis had great effect on the coalescence-induced droplet jumping. The larger advancing contact angle could improve the droplet jumping velocity, while the lower receding contact angle could reduce the droplet jumping velocity.

Acknowledgements

This work was financially supported by the Natural Science Foundation of China (Grant Nos: 51406050 and 51436004). YP Cheng would like to acknowledge the Marie Curie European Fellowship (Grant No. 658437).

References

[1] J.B. Boreyko, Y.J. Zhao, C.H. Chen, Planar jumping-drop thermal diodes, Appl. Phys. Lett. 99 (2011) 234105.
[2] N. Miljkovic, E.N. Wang, Condensation heat transfer on superhydrophobic surfaces, MRS Bull. 38 (2013) 397–406.
[3] N. Miljkovic, R. Enright, E.N. Wang, Modeling and optimization of superhydrophobic condensation, J. Heat Transfer 135 (2013) 111004.
[4] P.B. Whalley, Boiling, Condensation, and Gas–Liquid Flow, Oxford University Press, Oxford, England, 1987.
[5] H.X. Chen, J.L. Xu, Z.J. Li, F. Xing, J. Xie, W. Wang, W. Zhang, Flow pattern modulation in a horizontal tube by the passive phase separation concept, Int. J. Multiphase Flow 45 (2012) 12–23.
[6] H.X. Chen, J.L. Xu, Z.J. Li, F. Xing, J. Xie, Stratified two-phase flow pattern modulation in a horizontal tube by the mesh pore cylinder surface, Applied Energy 112 (2013) 1283–1290.
[7] J. Xie, J.L. Xu, F. Xing, Z.X. Wang, H. Liu, The phase separation concept condensation heat transfer in horizontal tubes for low-grade energy utilization, Energy 69 (2014) 787–800.
[8] Z. Cao, J.L. Xu, D.L. Sun, J. Xie, F. Xing, Q.C. Chen, X.D. Wang, Numerical simulation of modulated heat transfer tube in laminar flow Regime, Int. J. Therm. Sci. 75 (2014) 171–183.
[9] J. Chung, S. Kandlikar, Boiling and condensation, in: Multiphase Flow Handbook, CRC Press, 2005.
[10] B.L. Peng, X.H. Ma, Z. Lan, W. Xu, R.F. Wen, Analysis of condensation heat transfer enhancement with dropwise–filmwise hybrid surface. Droplet sizes effect, Int. J. Heat Mass Transfer 77 (2014) 785–794.
[11] J.B. Boreyko, C.H. Chen, Self-propelled jumping drops on superhydrophobic surfaces, Phys. Fluids 22 (2010) 091110.
[12] J.B. Boreyko, C.H. Chen, Self-propelled dropwise condensate on superhydrophbic surfaces, Phys. Rev. Lett. 103 (2009) 184501.
[13] C. Dorrer, J. Ruhe, Wetting of silicon nanograss: from superhydrophilic to superhydrophobic surfaces, Adv. Mater. 20 (2008) 159–163.
[14] J. Tian, J. Zhu, H.Y. Guo, J. Li, X.Q. Feng, X.F. Gao, Efficient self-propelling of small-scale condensed microdrops by closely packed ZnO nanoneedles, J. Phys. Chem. Lett. 5 (2014) 2084–2088.
[15] C.J. Lv, P.F. Hao, Z.H. Yao, Y. Song, X.W. Zhang, F. He, Condensation and jumping relay on lotus leaf, Appl. Phys. Lett. 103 (2013) 021601.
[16] N. Miljkovic, D.J. Preston, R. Enright, E.N. Wang, Electric-field-enhanced condensation on superhydrophobic nanostructured surfaces, ACS Nano 7 (12) (2013) 111043–111054.
[17] X.L. Liu, P. Cheng, X.J. Quan, Lattice Boltzmann simulations for self-propelled jumping of droplets after coalescence on a superhydrophobic surface, Int. J. Heat Mass Transfer 73 (2014) 195–200.
[18] X.L. Liu, P. Cheng, Lattice Boltzmann simulation for dropwise condensation of vapor along vertical hydrophobic flat plates, Int. J. Heat Mass Transfer 64 (2013) 1041–1052.
[19] X.L. Liu, P. Cheng, 3D multiphase lattice Boltzmann simulations for morphological effects on self-propelled jumping of droplets on textured superhydrophobic surfaces, Int. Commun. Heat Mass Transfer 64 (2015) 7–13.
[20] Y. Shi, G.H. Tang, H.H. Xia, Investigation of coalescence-induced droplet jumping on superhydrophobic surfaces and liquid condensate adhesion on slit and plain fins, Int. J. Heat Mass Transfer 88 (2015) 445–455.
[21] Y.S. Nam, H.S. Kim, S.W. Shin, Energy and hydrodynamic analysis of coalescence-induced jumping droplets, Appl. Phys. Lett. 103 (2013) 161601.
[22] Y.S. Nam, D.H. Seo, C.Y. Lee, S.W. Shin, Droplet coalescence on water repellent surfaces, Soft Matter 11 (2015) 154.
[23] F. Liu, G. Ghigliotti, J.J. Feng, C.H. Chen, Numerical simulations of self-propelled jumping upon drop coalescence on non-wetting surfaces, J. Fluid Mech. 752 (2014) 39–65.
[24] F.J. Liu, G. Ghigliotti, J.J. Feng, C.H. Chen, Self-propelled jumping upon drop coalescence on Leidenfrost surfaces, J. Fluid Mech. 752 (2014) 22–38.
[25] R. Enright, N. Miljkovic, J. Sprittles, K. Nolan, R. Mitchell, E.N. Wang, How coalescing droplets jump, ACS Nano 8 (10) (2014) 10352–10362.
[26] H. Ding, P.D.M. Spelt, Wetting condition in diffuse interface simulations of contact line motion, Phys. Rev. E 75 (2007) 046708.
[27] H. Ding, P.D.M. Spelt, C. Shu, Diffuse interface model for incompressible two-phase flows with large density ratios, J. Com. Phys. 226 (2007) 2078–2095.
[28] D. Jacqmin, Contact-line dynamics of a diffuse fluid interface, J. Fluid Mech. 402 (2000) 57–88.
[29] F.C. Wang, F.Q. Yang, Y.P. Zhao, Size effect on the coalescence-induced self-propelled droplet, Appl. Phys. Lett. 98 (2011) 053112.